Photonic band edge effects in finite structures and applications to $\chi^{(2)}$ interactions

G. D'Aguanno,[1,2] M. Centini,[1,2] M. Scalora,[2,3] C. Sibilia,[1] Y. Dumeige,[4] P. Vidakovic,[4] J. A. Levenson,[4] M. J. Bloemer,[2] C. M. Bowden,[2] J. W. Haus,[5] and M. Bertolotti[1]

[1]*INFM at Dipartimento di Energetica, Università di Roma ''La Sapienza,'' Via A. Scarpa, 16, I-00161 Rome, Italy*

[2]*U.S. Army Aviation and Missile Command, Weapons Sciences Directorate, AMSAM-RD-WS-ST, RD&E Center, Building 7804, Redstone Arsenal, Alabama 35898-5000*

[3]*Time Domain Corporation, Cummings Research Park, 7057 Old Madison Pike, Huntsville, Alabama 35806*

[4]*Laboratoire LPN (CNRS UPR 20), 196 Avenue Henri Ravera, 9220 Bagneux, France*

[5]*Electro-Optics Program, University of Dayton, Dayton, Ohio 45469-0245*

(Received 24 October 2000; revised manuscript received 7 December 2000; published 25 June 2001)

Using the concept of an effective medium, we derive coupled mode equations for nonlinear quadratic interactions in photonic band gap structures of finite length. The resulting equations reveal the essential roles played by the density of modes and effective phase matching conditions necessary for the strong enhancement of the nonlinear response. Our predictions find confirmation in an experimental demonstration of significant enhancement of second harmonic generation near the photonic band edge. The measured conversion efficiency is in good agreement with the conversion efficiency predicted by the effective-medium model.

DOI: 10.1103/PhysRevE.64.016609 PACS number(s): 42.70.Qs, 42.65.Ky, 42.25.Bs

I. INTRODUCTION

The past two decades have witnessed an intense investigation of electromagnetic wave propagation phenomena at optical frequencies in periodic structures. Usually referred to as photonic band gap (PBG) crystals [1], the essential property of these structures is the existence of allowed and forbidden frequency bands and gaps, in analogy with energy bands and gaps of semiconductors. Many applications have been envisioned in one-dimensional systems, which usually consist of multilayer, dielectric stacks, and include: a nonlinear optical limiter [2] and a diode [3]; a photonic band edge laser [4]; a true-time delay line for delaying ultrashort optical pulses [5]; a high-gain optical parametric amplifier for nonlinear frequency conversion [6]; and more recently, transparent metal-dielectric stacks [7] and all-optical switching [8]. Some demonstrations of the potential applications of these structures in higher dimensional systems have been highlighted recently with the realization of photonic crystal fibers [9], and in the microwave regime with the development of a PBG structure for applications to antenna substrates [10].

Second harmonic generation (SHG) has been experimentally observed under different circumstances. As an example, we cite the observation of SHG in a centrosymmetric, crystalline lattice of dielectric spheres [11]; in a semiconductor microcavity [12]; and near the band edge of a ZnS/SrF multilayer stack [13]. From a theoretical, more analytical point of view, the study of nonlinear optical interactions in PBG structures has been undertaken mainly in regard to solitonlike pulses (often referred to as gap-solitons) in cubic $\chi^{(3)}$ [14] and quadratic $\chi^{(2)}$ media [15]. One of the more intriguing aspects related to the $\chi^{(2)}$ response of PBG crystals that is of interest for a number of applications is the possibility of significantly increasing the conversion efficiency of nonlinear processes. We cite the enhancement of SHG as the simplest and well-known parametric nonlinear process, although in general our discussion is valid even for more complicated multiwave mixing processes [16]. The processes that we discuss owe their increased efficiency to the simultaneous availability of: (a) exact phase matching conditions [17]; and (b) high localization of the fields with frequencies tuned to transmission resonances near the photonic band edge.

Although it is generally agreed that phase matching conditions and strong field localization are responsible for the enhancement of nonlinear interactions near the band edge, here we set out to understand how these effects specifically influence nonlinear field dynamics in structures of finite length, i.e., with the introduction of entry and exit interfaces. The importance of the concept of the finiteness of the structure cannot be understated, and is reflected in the following conditions: the spatial extent of incident pulses may exceed the spatial extent of a typical structure by several orders of magnitude, as in Ref. [6]. The circumstances that arise in this case are not the same as those that are typically considered [14,15], where the structure is taken to be much longer compared to the spatial extent of the pulse.

The paper is organized as follows: in Sec. II we discuss the basic linear properties of 1D PBG structures of finite length, and we develop the effective-medium model. This approach will then be used in Sec. III, where we derive coupled mode equations for nonlinear quadratic interactions. Finally, in Sec. IV we report preliminary experimental results where enhanced SHG was observed for a 1D PBG structure composed of 37 periods of alternating $Ga_{0.7}Al_{0.3}As(135.1\,nm)/AlAs(106.4\,nm)$ layers. The experimental results are in good agreement with conversion efficiencies predicted by the effective-medium model.

II. THE PBG STRUCTURE AS AN ''OPEN CAVITY'': DENSITY OF MODES AND EFFECTIVE DISPERSION RELATION

Under the monochromatic plane-wave approximation, the Helmholtz equation for the evolution of the electric field in a lossless PBG structure is

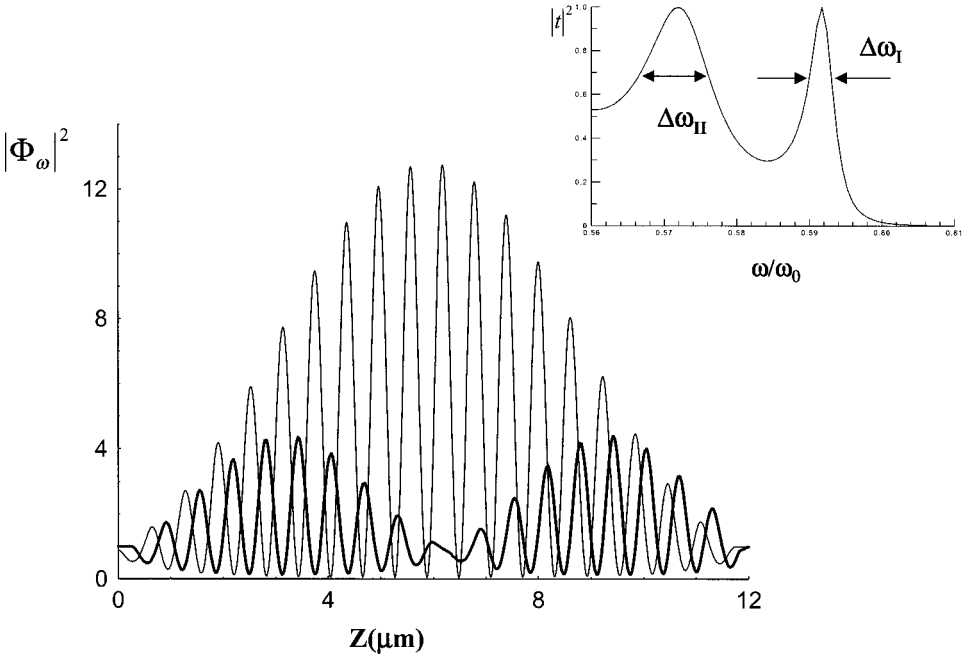

FIG. 1. Square modulus of the field distribution corresponding to the frequency that identifies the first transmission resonance (thin line), and the second transmission resonance (thick line) away from the band edge. Inset: the two band edge resonances, labeled as I and II, for a 20-period, 12-μm, half/quarter-wave stack. The indices of refraction are $n_a=1$ and $n_b=1.428\,57$. The layers have thicknesses $a=\lambda_0/(4n_a)$ and $b=\lambda_0/(2n_b)$, $\lambda_0=1\,\mu$m, $\omega_0=2\pi c/\lambda_0$.

$$\frac{d^2\Phi_\omega}{dz^2}+\frac{\omega^2\varepsilon_\omega(z)}{c^2}\Phi_\omega=0, \tag{1}$$

which is subject to the following boundary conditions at the input $(z=0)$ and output $(z=L)$ surfaces:

$$1+r_\omega=\Phi_\omega(0), \quad t_\omega=\Phi_\omega(L),$$

$$i\left(\frac{\omega}{c}\right)(1-r_\omega)=\frac{d\Phi_\omega(0)}{dz}, \quad i\left(\frac{\omega}{c}\right)t_\omega=\frac{d\Phi_\omega(L)}{dz}, \tag{2}$$

where $\varepsilon_\omega(z)$ is the spatially dependent, real dielectric permittivity function. For simplicity, in Eqs. (1) and (2) we have normalized the electric field with respect to the amplitude of the incident electric field by introducing the following dimensionless quantities: $\Phi_\omega(z)=E_\omega(z)/E^I_\omega$. Also, $t_\omega=(E^t_\omega/E^I_\omega)\exp[i(\omega/c)L]$, $r_\omega=E^r_\omega/E^I_\omega$; $\Phi_\omega(z)$ is the linear field distribution inside the stack, t_ω and r_ω are the coefficients of transmission and reflection, respectively. $E^I_\omega, E^r_\omega, E^t_\omega$ are the incident, reflected, and transmitted fields, respectively. These quantities can be numerically calculated using the standard matrix transfer technique.

Equation (1) and (2) describe a *non-Hermitian problem* because Eq. (1) is supplemented by boundary conditions at the input and output surfaces that give rise to a reflected and a transmitted wave from the structure. In other words, we are dealing with an *open cavity* problem [18]. Even if the field appears to become well localized *inside* the cavity, as shown in Fig. 1, for example, the field is never really confined in the true sense of the word because the field must first enter and eventually exit the structure. Thus, while the field distribution in Fig. 1 strongly resembles a bound-state function, a time-domain analysis of the problem shows that the wave first enters the structure, gives rise to a highly localized, *metastable state* [19(a)], and then slowly leaks out through the input and output surfaces as shown in Figs. 2. As a result, the problem does not admit true eigenstates intended in the traditional sense of the word, i.e., a complete basis of expansion in the space between $z=0$ and $z=L$ [20]. Nevertheless, the problem admits metastable, or quasistationary states that by virtue of their localization properties can be associated with an effective density of modes (DOM). One way to define a proper DOM for structures of finite length is to resort to the spatially averaged electromagnetic energy density. For the field distribution $\Phi_\omega(z)$, which is expressed in dimensionless units, we define the DOM as (see the Appendix)

$$\rho_\omega\equiv\frac{1}{2Lc}\int_0^L\left[\varepsilon_\omega(z)|\Phi_\omega|^2+\frac{c^2}{\omega^2}\left|\frac{d\Phi_\omega}{dz}\right|^2\right]dz. \tag{3}$$

In general, the DOM should reflect the localization properties of the field inside the structure. Integrating Eq. (3) by parts, we note that the second term on the right-hand side is

$$\int_0^L|d\Phi_\omega/dz|^2dz=(\omega/c)^2\int_0^L\varepsilon_\omega(z)|\Phi_\omega|^2dz - (2\omega/c)\mathrm{Im}(r_\omega).$$

Consequently, the expression for the DOM in Eq. (3) takes on the following, more suggestive form:

$$\rho_\omega=\frac{1}{Lc}\int_0^L\varepsilon_\omega(z)|\Phi_\omega|^2dz-\frac{1}{\omega L}\mathrm{Im}(r_\omega). \tag{4}$$

From Eq. (4), it is clear that the DOM is directly linked to the localization properties of the field distribution of the metastable state $\Phi_\omega(z)$ inside the PBG structure.

In Fig. (3), we compare our definition of the DOM with the definition given in Ref. [21], namely, $\rho_\omega\equiv(1/L)(d\varphi_t/d\omega)$, where $\varphi_t(\omega)$ is the phase of the transmission

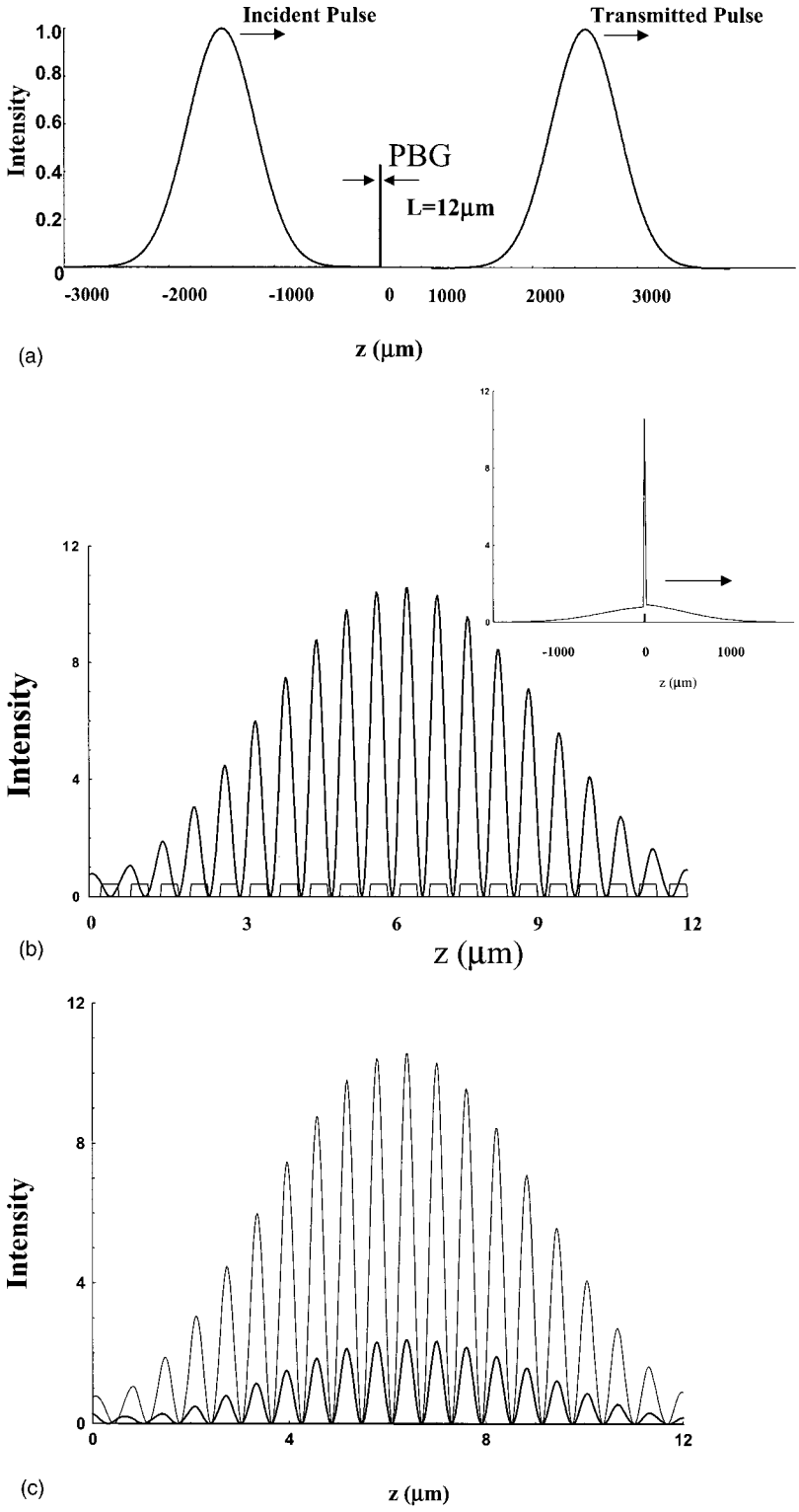

FIG. 2. (a) 2-ps incident and transmitted Gaussian pulses with unit incident amplitude, with carrier frequency tuned at the first transmission resonance of the PBG structure. The spectral bandwidth of the pulse is much narrower with respect to the bandwidth of the transmission resonance. Note that spatial extent of the pulse with respect to structure length is to scale. (b) Internal field profile when the peak of the pulse reaches the structure. Inset: the pulse is shown in its entirely. The large spike visible in the inset corresponds to the field profile of the figure. Note that most of the pulse is located outside the structure. (c) Metastable states for 2-ps [Fig. 2(b)] (thin line) and for the 200-fs pulses (thick line). The longer pulse is much more localized than the shorter pulse due to its narrower frequency bandwidth.

function, defined as $t_\omega = |t_\omega| \exp[i\varphi_t(\omega)]$. These two very different formulations of the DOM yield the same results in the passband, and show only modest quantitative departures inside the band gap (see inset of Fig. 3). Although quantitative differences are slight, our definition given in Eq. (3) is more appealing from a physical and a conceptual point of view because, contrary to the definition given in Ref. [21] in terms of the transmission function, it establishes a clear direct link between the localization properties of the metastable states and the concept of DOM. Once the DOM ρ_ω has been defined in Eq. (3), it is then possible to find an *effective dispersion relation* for a generic, finite structure, not necessarily multilayered, in an *unambiguous way* [22]. The real part of the effective dispersion relation $k_r(\omega)$ is the solution of the following first-order linear differential equation: $dk_r(\omega)/d\omega = \rho_\omega$, supplemented by the initial condition

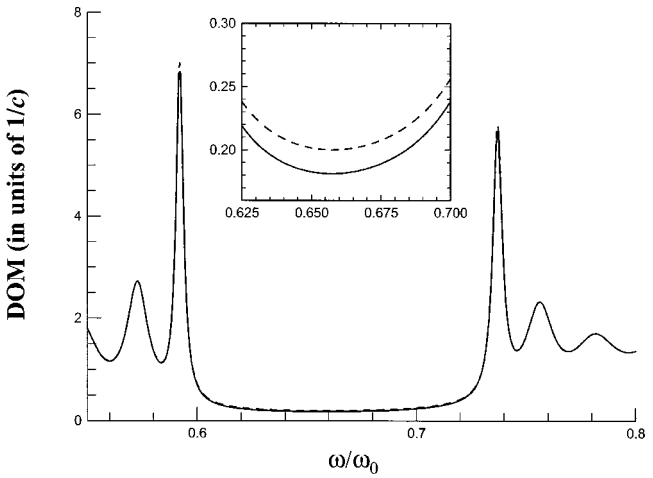

FIG. 3. Density of modes for the PBG structure described in the caption of Fig. 1 calculated using Eq. (3) (solid line) and using the phase of the transmission function (dotted line). Inset: inside of the gap is magnified. The difference is about 10% at center gap.

$k_r(0)=0$. The imaginary part of the dispersion relation is calculated by invoking the causality principle through the Kramers-Kronig relations:

$$k_I(\omega)=-(2/\pi)\mathrm{P}\int_0^\infty [\Omega k_r(\Omega)/(\Omega^2-\omega^2)]d\Omega.$$

From the effective dispersion relation $\hat{k}(\omega)=k_r(\omega)+ik_I(\omega)$, we can also introduce an effective index as [22]: $\hat{k}(\omega)=(\omega/c)\hat{n}_{\mathrm{eff}}(\omega)=(\omega/c)[n^r_{\mathrm{eff}}(\omega)+in^I_{\mathrm{eff}}(\omega)]$. Both real and imaginary parts of the effective index of refraction are plotted in Figs. 4(a)–4(b) for a 2- and a 20-period structure, and compared with the dispersion relation of the infinite structure.

III. $\chi^{(2)}$ INTERACTIONS AND THE EFFECTIVE MEDIUM APPROACH

In addition to the full numerical integration of Maxwell's equations to solve for the nonlinear dynamics in a PBG structure [6], other approaches also exist in the form of more approximate solutions: a Green's function approach [23(a)], and a coupled mode theory [23(b)], in the case of shallow gratings; a Bloch mode expansion for periodic gratings of arbitrary deep [24]. In this work we propose a simple and elegant approach based on our effective-medium model that gives a direct estimate of the conversion efficiency when strong localization effects and the appearance of metastable states of the kind discussed above come into play. *The method that we propose can be applied to any generic linear index profile provided spectral band shifts do not occur* [25]. The effective index approach can simplify the problem of calculating the conversion efficiency of $\chi^{(2)}$ interactions in PBG structures because in this picture the fields ''see'' an effective bulk material with a well-defined dispersion relation.

We write the coupled mode equations for nonlinear quadratic interactions in a finite PBG structure of length L *as if*

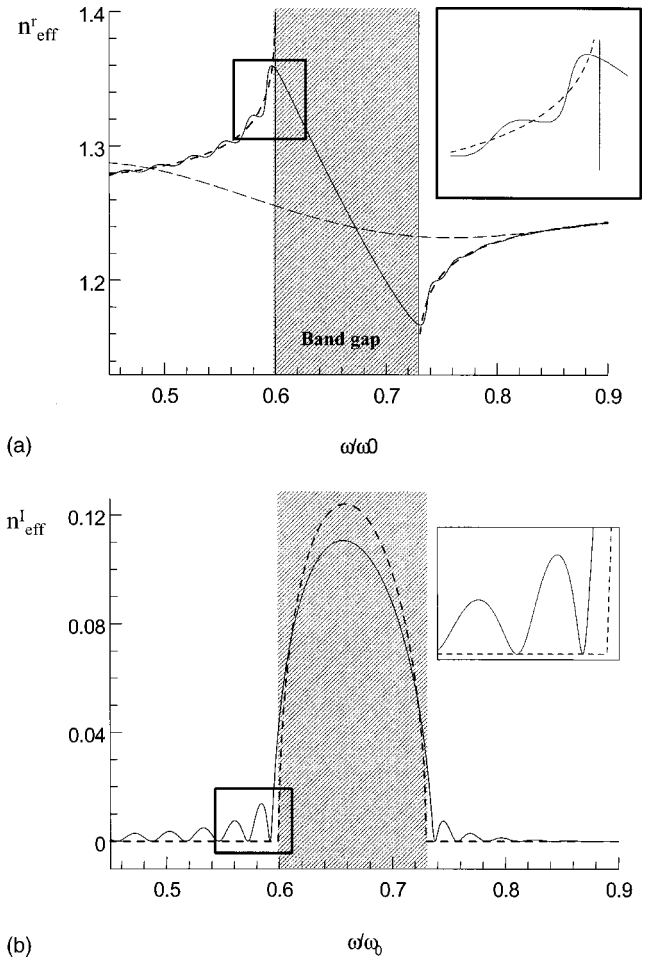

FIG. 4. (a) Real part of the effective index for a 2-(long dashes) and 20-period (solid curve) structure; dispersion relation for the infinite structure (short dashes). In the inset the band edge is magnified. (b) Imaginary part of the effective index, same as Fig. 4(a), without the 2-period curve. The real part of the index displays anomalous dispersion inside the gap and between resonances. The imaginary component is identically zero at each transmission resonance.

the interaction were taking place in a bulk material of the same length L, but with an effective dispersion relation as described in Sec. II. In the case of two monochromatic waves at fundamental frequency (FF) ω and second harmonic frequency (SH) 2ω, each tuned at a peak of transmittance where the imaginary part of the effective dispersion relation is zero [17], the coupled mode equations written for the effective medium are

$$\frac{dA_\omega}{dz}=i\frac{\omega}{n^r_{\mathrm{eff}}(\omega)c}d_{\mathrm{eff}}A_{2\omega}A^*_\omega\exp[i\Delta k_{\mathrm{eff}}z], \tag{5a}$$

$$\frac{dA_{2\omega}}{dz}=i\frac{\omega}{n^r_{\mathrm{eff}}(2\omega)c}d_{\mathrm{eff}}A^2_\omega\exp[-i\Delta k_{\mathrm{eff}}z], \tag{5b}$$

where $\Delta k_{\mathrm{eff}}=k_r(2\omega)-2k_r(\omega)$ is the *effective phase mismatch* calculated using the real part of the effective dispersion re-

lation; $n_{\rm eff}^r$ is the real part of the effective index; and $d_{\rm eff}$ is the *effective nonlinear coupling coefficient* defined as

$$d_{\rm eff}=\frac{1}{L}\int_0^L d^{(2)}(z)|\Phi_\omega(z)|^2|\Phi_{2\omega}(z)|dz, \tag{6}$$

where $d^{(2)}(z)$ is the quadratic coupling function. It is overlapped with the square modulus of the linear FF field and the modulus of linear field at the SH frequency, both calculated using Eqs. (1) and (2). For second harmonic generation in the undepleted pump approximation, we obtain the expression for the conversion efficiency η in analogy with the conversion efficiency calculated for bulk materials,

$$\eta=\frac{8\pi^2 d_{\rm eff}^2 L^2 \tilde{I}_p}{[n_{\rm eff}^r(\omega)]^2 n_{\rm eff}^r(2\omega)\varepsilon_0 c\lambda^2}\,{\rm sinc}^2\left(\frac{\Delta k_{\rm eff}L}{2}\right), \tag{7}$$

where $\tilde{I}_p=(\frac{1}{2})\varepsilon_0 c n_{\rm eff}^r(\omega)|A_\omega|^2$ is the scaled input pump intensity. From Eq. (4), at the peak of transmittance $\rho_\omega=(1/Lc)\int_0^L \varepsilon_\omega(z)|\Phi_\omega|^2 dz$. As a consequence, $d_{\rm eff}$ is enhanced by a factor proportional to the DOM when the FF field is localized inside the nonlinear layers, $d_{\rm eff}\propto\rho_\omega d_{\rm layer}^{(2)}$, where $d_{\rm layer}^{(2)}$ is the actual second-order susceptibility of the nonlinear layer. Therefore, we expect an enhancement of the conversion efficiency approximately proportional to ρ_ω^2.

In order to draw meaningful comparisons with an appropriate bulk material we can define, from Eq. (7), a figure of merit $\mathcal{F}^{\rm merit}$ as:

$$\mathcal{F}^{\rm merit}=L^2\left(\frac{d_{\rm eff}}{d_{\rm layer}^{(2)}}\right)^2 {\rm sinc}^2\left(\frac{L}{2L_c}\right), \tag{8}$$

where $L_c=1/\Delta k_{\rm eff}$ is either one coherence length in the case of bulk material or the effective coherence length ($L_c^{\rm eff}$) calculated via the real effective index $n_{\rm eff}^r$ in the case of a PBG structure.

Now that we have developed all the major components of the model, we mention its fundamental limitations. Coupled mode equations (5) cannot give detailed information about the actual nonlinear dynamics of the fields inside the structure. This is evident if we recall that our approach to the problem consists in substituting the finite PBG structure with an equivalent length of bulk material and an effective dispersion relation. As a result, we cannot expect that this model will yield both a reflected and a transmitted component. However, the solutions of Eqs. (5) yield remarkably accurate energy conversion efficiencies when compared to the conversion efficiencies calculated by numerically integrating the nonlinear coupled Maxwell's equations [6]. In Fig. (5) we calculate the SH conversion efficiency for a multilayer stack [see caption of Fig. (5)]. The structure was designed to satisfy the perfect phase matching conditions in the sense of the effective index: $\Delta k_{\rm eff}=0$, with the pump incident at an angle of 30° with respect to the surface of the structure. We find a conversion efficiency of approximately 15% in a single pass through the device, with input power levels of 40 GW/cm^2. To test the validity of the effective-medium model, in Fig. (6) we plot the results of a numerical integration carried out

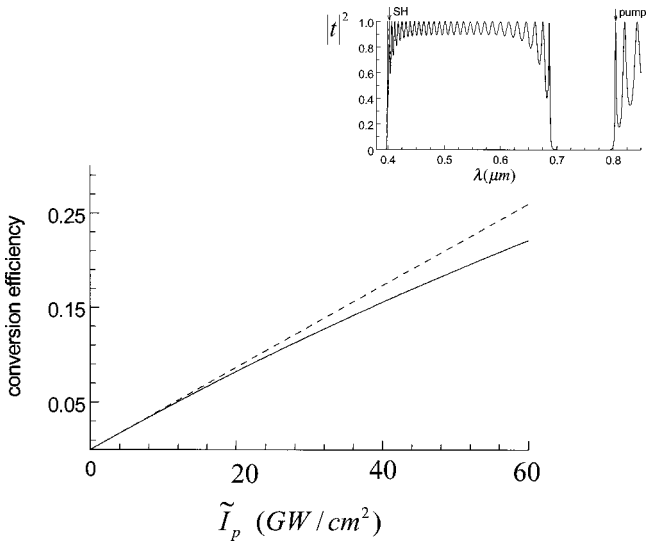

FIG. 5. Second harmonic conversion efficiency vs the input pump intensity in the undepleted pump approximation (dotted line) and in the case of pump depletion (continuous line). A conversion efficiency of approximately 15% is reached for input pump intensity of 40 GW/cm^2. Inset: Transmittance for a 30-period, 6-μm, SiO_2/AlN, quarter-wave/half-wave stack. The reference wavelength is 0.53 μm. The FF (800 nm) and SH (400 nm) fields are tuned to the first transmission resonance near the first-order band gap and to the second resonance near the second-order gap, respectively.

as discussed in Ref. [6]. The conversion efficiency obtained numerically is approximately equal to what the effective-medium model predicts.

IV. EXPERIMENTAL RESULTS

We now demonstrate SH enhancement due to an increase of the density of modes and to the effective phase matching conditions discussed above. We designed and fabricated a 1D semiconductor structure, grown by metallorganic

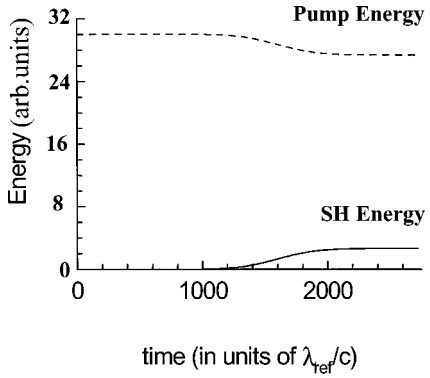

FIG. 6. Energy converted from the pump to the SH field as function of the time. $\lambda_{\rm ref}$ corresponds to a wavelength of 1 μm. We pump with a 2-ps pulse incident from the left, with 40 GW/cm^2 of peak input intensity. The conversion efficiency, given by the amount of energy converted to SH divided the total amount of initial energy in the FF, is approximately $(4/30)\approx 13\%$, in good agreement with that predicted by the effective-medium model.

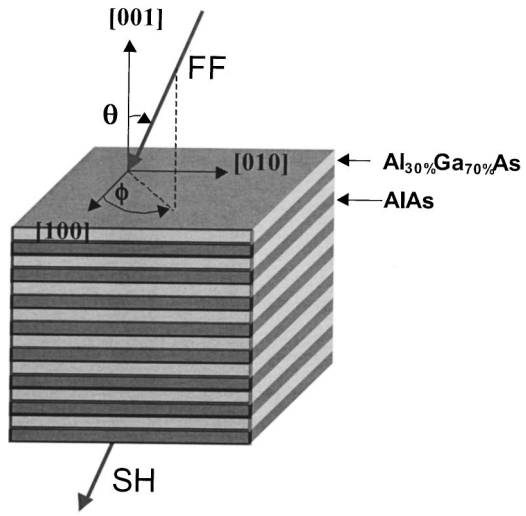

FIG. 7. Schematic view of the experimental, semiconductor sample. The incidence (θ) and azimuthal (ϕ) angles are also represented together with the crystal axis.

vapor-phase epitaxy on a GaAs substrate, composed of 37 periods of $Ga_{0.7}Al_{0.3}As(135.1\,nm)/AlAs(106.4\,nm)$. The $Ga_{0.7}Al_{0.3}As$ and AlAs refractive indices are $n_\omega = 3.231$ and 2.902 at FF wavelength, and $n_{2\omega} = 3.4662$ and 3.0149 at the SH wavelength, respectively. The details of the experiment will be reported elsewhere [26]. Here we give a brief overview of the results. The structure was grown on the usual [001] direction, and designed for operation at an oblique incidence angle. Indeed, the high $\bar{4}3m$ symmetry of III-V zinc-blende semiconductors leaves only one nonlinear coefficient (d_{14}) for the second-order susceptibility. Though this coefficient is extremely large (120 pm/V for GaAs), one important consequence of the symmetry rules is that second-order processes are forbidden along the three crystal axes of widely used substrate orientations for mature epitaxy technology on GaAs (that is, [100], [010], and [001]). A solution consists of sending the laser beam on the structures at an oblique angle. For a FF external angle of 10° with respect to the stack axis, the $Ga_{0.7}Al_{0.3}As$ effective $\chi^{(2)}$ is of the order of 13 pm/V, and almost zero in the AlAs layers. This external angle corresponds to a very small internal angle ($\sim 3°$) for which the PBG's FF resonances are almost identical for incident TM and TE polarized fields. As we will see in the following, this allows us to directly test the influence of the effective phase matching conditions by comparing the performance of the PBG operated for a TM- or a TE-polarized FF wavelength.

Figure (7) depicts the geometry of the air/PBG/air suspended sample as well as the FF angle incidence with respect to the crystallographic axis. We recall that for an azimuthal angle $\phi = \pi/4$ (azimuth corresponding to the angle between [100] crystal axis and the projection of the wave vector on the (001) plane) only TM→TM and TE→TM interactions are allowed by the symmetry of the $\chi^{(2)}Ga_xAl_{1-x}As$ tensor.

Figure (8) (upper traces) depicts the expected (solid line) and measured (dotted line) transmissions for TM polarization around the FF and SH wavelength. Stop bands are clearly visible near 1.52 and 0.79 μm. The arrows indicate the operating FF (1.55 μm) and SH (0.775 μm) wavelengths. The

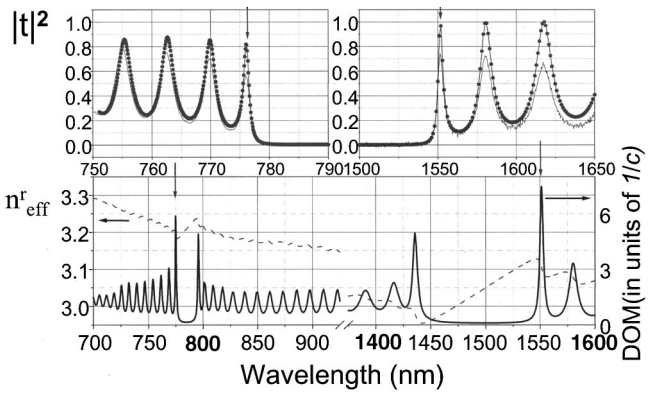

FIG. 8. Top view calculated (dotted lines) and measured (solid lines) transmission spectra around the fundamental and the second harmonic wavelength (indicated by vertical arrows). Bottom view: inferred DOM (full line) and effective refraction index (dashed lines).

lower curve depicts the calculated DOM (solid lines), normalized to the DOM corresponding to one coherence length of $Ga_{0.7}Al_{0.3}As$, for a TM-polarized FF. The expected DOM enhancement is 7.1 for FF and 4.5 for the SH. Note that, as already stressed, these values are close to those expected for a TE polarized FF (6.8 and 4.3, respectively). The dispersion of the effective refractive index is represented as well for a TM polarized F (dashed lines). The effective refractive indices are $n^{r,\mathrm{TM}}_{\mathrm{eff},F} = 3.1539$ and $n^{r,\mathrm{TE}}_{\mathrm{eff},F} = 3.1584$ for the FF, and $n^{r,\mathrm{TM}}_{\mathrm{eff,SH}} = 3.2362$ and $n^{r,\mathrm{TE}}_{\mathrm{eff,SH}} = 3.2355$ for the SH. It becomes clear that under the present experimental conditions, material dispersion is too high to be fully compensated with geometrical dispersion alone. Nevertheless, an appreciable change (by almost a factor of 3) on the effective coherence length L_c^{eff} is obtained with respect to the original one. Moreover, this change is different for a TM- or a TE-polarized FF wavelength: $L_c^{\mathrm{TM,eff}} = 2.86 L_c$ and $L_c^{\mathrm{TE,eff}} = 3.03 L_c$. This gives a direct way, without the need of any external calibration, of testing the effective parameter theory.

From these considerations, and using Eq. (8), we expect enhancement factors of

$$\left(\frac{\mathcal{F}^{\mathrm{merit}}_{\mathrm{PBG}}}{\mathcal{F}^{\mathrm{merit}}_{Lc}}\right)^{\mathrm{TM}\to\mathrm{TM}} = 10.8 \quad \text{and} \quad \left(\frac{\mathcal{F}^{\mathrm{merit}}_{\mathrm{PBG}}}{\mathcal{F}^{\mathrm{merit}}_{L_c}}\right)^{\mathrm{TE}\to\mathrm{TM}} = 68.4$$

with respect to one coherence length of nonlinear material. $\mathcal{F}^{\mathrm{merit}}_{L_c}$ is the figure of merit for one coherence length of $Ga_{0.7}Al_{0.3}As$. While the TM-polarized FF wavelength DOM is comparable to that for the TE polarization, the figure of merit is significantly *greater* for a TE polarized FF wavelength than for the TM. The TE→TM process owes its increased efficiency with respect to the TM→TM process primarily to the smaller mismatch in the effective index ($\Delta n^r_{\mathrm{eff}} = 0.0778$ for TE→TM to be compared to $\Delta n^r_{\mathrm{eff}} = 0.0823$ for the TM→TM case).

In the experiments we used 8-ps pulses generated by a mode-locked fiber-laser, with 20-MHz repetition rate. The laser source is tunable between 1.53 and 1.56 μm. Figure 9 represents the second harmonic intensity as a function of the

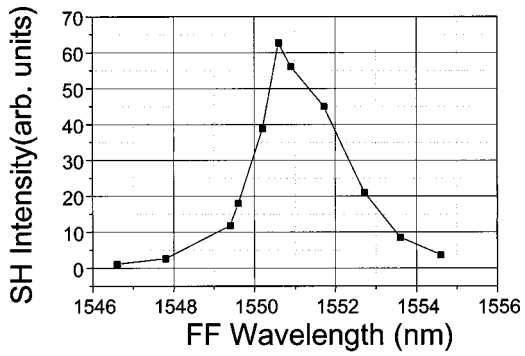

FIG. 9. Second harmonic intensity as a function of the fundamental wavelength. Fundamental is polarized TM and $\theta = 10°$.

FF wavelength. The FF wavelength is TM polarized, with a mean power of 30 mW. The external and the azimuthal angles are $\theta = 10°$ and $\phi = \pi/4$, respectively. The spectral width of the generated SH is comparable to the bandwidth of the SH resonance, clearly demonstrating the effect of PBG double resonance. Figure 10 represents, in a semilogarithmic scale, the SH signal generated in transmission with a TM (filled circles) and a TE (filled squares) polarized FF wavelength, as a function of the fundamental power. Both curves follow the expected quadratic behavior. Also represented is the SH signal generated by one coherence length of $Ga_{0.7}Al_{0.3}As$ under identical geometrical conditions (TM is in open circles, and TE in open squares). The FF azimuthal angle is $\phi = \pi/4$. The measured enhancement is ten times (50 times) for TM (TE) incident FF wavelength, in good agreement with the theoretical prediction.

The good agreement obtained between the experimental results and the theoretical predictions, for an azimuthal angle of $\phi = \pi/4$, clearly shows that the higher DOM and the effective coherence length are responsible for the observed enhancement of SH in the PBG. The role that the DOM plays was furthermore emphasized by a comparison of present results and experiments performed on the same sample using 100-fs incident pulses. In contrast to the 8-ps long pulses, the shorter pulses have bandwidths much larger than the PBG resonance bandwidth and effects due to field localization and

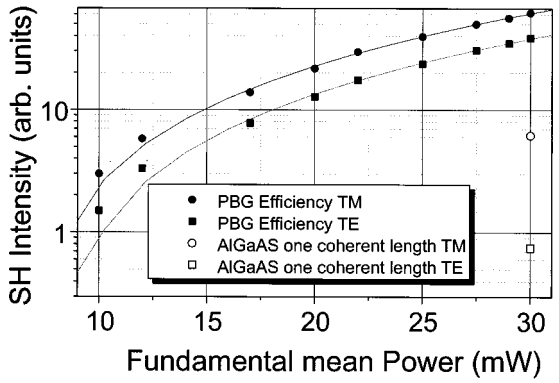

FIG. 10. Second harmonic intensity as a function of fundamental power. Filled circles (squares) correspond to a TM (TE) polarized fundamental. Also indicated are the values for 1 $Ga_{0.7}Al_{0.3}As$ coherence length.

effective nonlinear gain are strongly attenuated [6], as discussed in earlier sections and in Fig. 2(b). In addition, experiments performed under a different azimuthal angle demonstrate clearly that surface and interface second harmonic generation are negligible, and constitute additional proof that the observed enhancement [26] of second harmonic generation is primarily due to the simultaneous availability of high mode density and change of coherence length near the band edge.

V. CONCLUSIONS

In summary, we have analyzed the properties of nonlinear quadratic interactions near the photonic band edge by studying the linear properties of finite PBG structures and by using the concept of an effective medium. We arrive at nonlinear coupled mode equations that are formally similar to the equations for quadratic interactions in bulk materials, scaled by the appropriate coupling coefficients that define the multilayer stack. These equations predict energy conversion rates that are in agreement with those predicted by an integration of the coupled wave equations in the time domain, and with the experimental results. Both theory and experiment suggest that enhancement effects near the band edge are entirely due to the simultaneous availability of field localization (high density of modes) and the engineering of the phase matching conditions. In our view, these unusual circumstances make PBG structures the best candidates for micron-sized nonlinear frequency converters based on quadratic nonlinearities.

ACKNOWLEDGMENTS

Two of us (G.D. and M.C.) are grateful to the U.S. Army European Research Office for financial support. This work was also supported by the OPEN Esprit project ANLM.

APPENDIX

The definition of DOM given in our Eq. (3) can be justified in analogy with the quantum mechanical properties of massive particles. The probability that a quantum particle can be found with a momentum between $\hbar k$ and $\hbar(k+dk)$ is given by

$$dP(k) = \Psi(k)\Psi^*(k)dk, \tag{A1}$$

where $\Psi(k)$ is the wave function of the quantum particle in the momentum representation. Mapping Eq. (A1) into the frequency domain can be accomplished with knowledge of the dispersion relation. That is, if $k = k(\omega)$, the mapping $P(k) \rightarrow p(\omega)$, $\Psi(k) \rightarrow \psi(\omega)$ leads to

$$dp(\omega) = \psi(\omega)\psi^*(\omega)\rho_\omega d\omega, \tag{A2}$$

where $\rho_\omega = (dk/d\omega)$ is the DOM. From Eq. (A2) we formally obtain the expression for the DOM in the following form:

$$\rho_\omega = \frac{\frac{dp(\omega)}{d\omega}}{|\psi(\omega)|^2}. \tag{A3}$$

Note that $dp(\omega)$ is only *proportional*, and not equal, to the probability that a quantum particle can be found with an energy between $\hbar\omega$ and $\hbar(\omega+d\omega)$ because in general the mapping of the functions from k space into the frequency domain via the dispersion relation $k=k(\omega)$ does not correspond to a unitary transformation.

Following Bohm [19b], in the case of classical electromagnetic fields, i.e., when many quanta of light are excited in a coherent state and the classical limit is approached [27], we may resort to the *electromagnetic energy density* that in this case plays a role analogous to the role played by the probability density in the case of massive, quantum particles. In fact, in the classical limit, the electromagnetic energy density U_ω is proportional to the mean number of photons in the range from ω to $(\omega+d\omega)$ [19b]. Keeping these considerations in mind, we express the DOM for the finite 1-D PBG structure as the spatially averaged electromagnetic energy density, which in our case plays a role analogous $dp(\omega)/d\omega$, as in Eq. (A3). The normalization factor found in Eq. (A3), $|\psi(\omega)|^2$, is then replaced by the energy density of the incident field $c|E^I_\omega|^2$. We therefore write the DOM as

$$\rho_\omega = \frac{\frac{1}{2L}\int_0^L \left[\varepsilon_\omega(z)|E_\omega|^2 + \frac{c^2}{\omega^2}\left|\frac{dE_\omega}{dz}\right|^2\right]dz}{c|E^I_\omega|^2}. \tag{A4}$$

Introducing the dimensionless field distribution inside the PBG structure as $\Phi_\omega(z)=E_\omega(z)/E^I_\omega$, we obtain,

$$\rho_\omega = \frac{1}{2Lc}\int_0^L \left[\varepsilon_\omega(z)|\Phi_\omega|^2 + \frac{c^2}{\omega^2}\left|\frac{d\Phi_\omega}{dz}\right|^2\right]dz, \tag{A5}$$

that is, the definition of DOM we give in Eq. (3) in the text.

[1] P. Yeh, *Optical Waves in Layered Media* (Wiley, New York, 1988); E. Yablonovitch, Phys. Rev. Lett. **58**, 2059 (1987); S. John, *ibid.* **58**, 2486 (1987); J. Maddox, Nature (London) **348**, 481 (1990); E. Yablonovitch and K. M. Leung, *ibid.* **351**, 278 (1991); J. Martorell and N. M. Lawandy, Phys. Rev. Lett. **65**, 1877 (1990); J. Opt. Soc. Am. B **10**, 279 (1993); J. Mod. Opt. **41**, 171 (1994); J. D. Joannopoulos, R. D. Mead, and J. N. Winn, *Photonic Crystals* (Princeton University Press, Princeton, 1994); G. D'Aguanno, M. Centini, M. Scalora, C. Sibilia, M. J. Bloemer, C. M. Bowden, J. W. Haus, and M. Bertolotti, Phys. Rev. E **63**, 036610 (2001).

[2] M. Scalora, J. P. Dowling, C. M. Bowden, and M. J. Bloemer, Phys. Rev. Lett. **73**, 1368 (1994).

[3] M. Scalora, J. P. Dowling, M. J. Bloemer, and C. M. Bowden, J. Appl. Phys. **76**, 2023 (1994).

[4] J. P. Dowling, M. Scalora, M. J. Bloemer, and C. M. Bowden, J. Appl. Phys. **75**, 1896 (1994).

[5] M. Scalora, R. J. Flynn, S. B. Reinhardt, R. L. Fork, M. D. Tocci, M. J. Bloemer, C. M. Bowden, H. S. Ledbetter, J. M. Bendickson, J. P. Dowling, and R. P. Leavitt, Phys. Rev. E **54**, 1078 (1996).

[6] M. Scalora, M. J. Bloemer, A. S. Manka, J. P. Dowling, C. M. Bowden, R. Viswanathan, and J. W. Haus, Phys. Rev. A **56**, 3166 (1997).

[7] M. Scalora, M. J. Bloemer, A. S. Pethel, J. P. Dowling, C. M. Bowden, and A. S. Manka, J. Appl. Phys. **83**, 2377 (1998).

[8] G. D'Aguanno, E. Angelillo, C. Sibilia, M. Scalora, and M. Bertolotti, J. Opt. Soc. Am. B **17**, 1188 (2000).

[9] J. C. Knight, T. A. Birkes, P. St. Russel, and J. P. De Sandro, J. Opt. Soc. Am. A **15**, 748 (1998).

[10] E. Yablonovitch, Microwave J. **VI**, 66 (1999).

[11] J. Martorell, R. Vilaseca, and R. Corbalan, Appl. Phys. Lett. **70**, 702 (1997); J. Martorell, R. Vilaseca, R. Corbalan, Phys. Rev. A **55**, 4520 (1997).

[12] C. Simonneau, J. P. Debray, J. C. Harmand, P. Vidakovic, D. J. Lovering, and J. A. Levenson, Opt. Lett. **23**, 1775 (1997).

[13] A. V. Balakin, D. Boucher, V. A. Bushev, N. I. Koroteev, B. I. Mantsyzov, P. Masselin, I. A. Ozheredov, and A. P. Shurinov, Opt. Lett. **24**, 793 (1999).

[14] W. Chen and D. L. Mills, Phys. Rev. Lett. **58**, 160 (1987); J. E. Sipe and H. G. Winful, Opt. Lett. **13**, 132 (1988); S. John and N. Akozbek, Phys. Rev. Lett. **71**, 1168 (1993); C. M. de Sterke, D. G. Salinas, and J. E. Sipe, Phys. Rev. E **54**, 1969 (1996); B. J. Eggleton, R. E. Slusher, C. M. de Sterke, P. A. Krug, and J. E. Sipe, Phys. Rev. Lett. **76**, 160 (1996).

[15] C. Conti, S. Trillo, and G. Assanto, Phys. Rev. Lett. **78**, 2341 (1997).

[16] G. D'Aguanno, M. Centini, C. Sibilia, M. Bertolotti, M. Scalora, M. Bloemer, and C. M. Bowden, Opt. Lett. **24**, 1663 (1999).

[17] M. Centini, C. Sibilia, M. Scalora, G. D'Aguanno, M. Bertolotti, M. Bloemer, C. M. Bowden, and I. Nefedov, Phys. Rev. E **60**, 4891 (1999).

[18] A. E. Siegman, Phys. Rev. A **39**, 1253 (1989); P. T. Leung, W. M. Suen, C. P. Sun, and K. Young, Phys. Rev. E **57**, 6101 (1998).

[19] (a) D. Bohm *Quantum Theory* (Dover, New York, 1989), pp. 283–295; (b) *ibid.* pp. 97–98.

[20] The open system that we discuss should be compared with a one-dimensional, *Hermitian* boundary value electromagnetic problem. The hermiticity is a direct consequence of energy conservation within the space $z=0$ and $z=L$. In fact, when the energy is conserved within the space $z=0$ and $z=L$, we can use periodic boundary conditions without loss of generality. Periodic boundary conditions ensure the hermiticity of the electromagnetic problem and allow us to calculate the number of modes (eigenfunctions) per unit frequency range in a straightforward manner, namely, $N(\omega)=(L/\pi)\rho_\omega$, where $\rho_\omega = (dk/d\omega)$ is the DOM, and $k(\omega)$ gives the range of allowed wave vectors. In fact, the dispersion relation can be obtained by formally connecting the spectrum of eigenfrequencies $\{\omega_n\}$

to their corresponding spectrum of wave-vectors $\{k_n \sim n\pi/L\}$, $n=1,2,3,\ldots$.

[21] (a) J. M. Bendickson, J. P. Dowling, and M. Scalora, Phys. Rev. E **53**, 4107 (1996); (b) C. Sibilia, I. Nefedov, M. Bertolotti, and M. Scalora, J. Opt. Soc. Am. B **15**, 1947 (1998).

[22] In Ref. [17] we derived the effective index for the finite structure using the phase of the transmission function. However, the work in Ref. [17] suffered by one serious ambiguity. While the effective index calculated by the phase of the transmission function was *uniquely* defined, it was not possible to identify a unique effective index calculated using the phase of the reflection function. The two indices converged only for structures of infinite length. This ambiguity is clearly removed in the present procedure because we arrive at a unique definition of the effective index for the finite PBG structure. This effective index corresponds to the effective index calculated in Ref. [17] using the phase of the transmission function.

[23] (a) M. J. Steel and C. M. de Sterke, Appl. Opt. **35**, 3211 (1996); (b) J. W. Haus, R. Viswanathan, M. Scalora, A. G. Kalocsai, J. D. Cole, and J. Theimer, Phys. Rev. A **57**, 2120 (1998), and references therein.

[24] C. M. de Sterke and J. E. Sipe, Phys. Rev. A **38**, 5149 (1988); A. Arraf and C. M. de Sterke, Phys. Rev. E **58**, 7951 (1998), and references therein.

[25] Spectral shifts can generally be neglected if the linear index step is much larger than any nonlinear index change. The typical index discontinuity that we consider is of order unity, while typical nonlinear index changes are some three orders of magnitude smaller.

[26] Y. Dumeige, P. Vidakovic, S. Sauvage, I. Sagnes, J. A. Levenson, C. Sibilia, M. Centini, G. D'Aguanno, and M. Scalora, Appl. Phys. Lett. **78**, 3021 (2001).

[27] R. Loudon, *The Quantum Theory of Light*, 2nd ed. (Oxford University Press, Oxford, 1984).